willow as well (*13*). The *p*H was usually in the range 5.5 to 7, although two samples had *p*H <5 with [S(IV)] less than 10 μM. HMSA was not determined in all the samples from Buttonwillow, but little or none was observed in the samples that were analyzed. As noted above, the lifetime of HMSA at *p*H 5.6 is 25 hours and should decrease further as *p*H rises. Thus HMSA may decompose during advection from SO_2 source areas to Buttonwillow. More HMSA and S(IV) is observed at Bakersfield because of its proximity to the oil fields in Oildale. If the atmosphere in the valley were not buffered by NH_3 emissions, then HMSA would have a longer residence time.

The results of this study support the hypothesis that HMSA may be an important species in fog and cloud water. The pattern of [HMSA] in the fog samples is consistent with the formation of HMSA during favorable conditions of high SO_2 and intermediate *p*H and preservation by subsequent acidification. Over the *p*H range of 5.5 to 7, which is typical of the samples from the San Joaquin Valley, the chemical lifetime of HMSA is shorter than the time for atmospheric transport within the valley (*19*). Appreciable [HMSA] or [S(IV)] was not observed at Buttonwillow. Observations of excess [S(IV)] and [CH_2O] in fog and cloud water from the more acidic Los Angeles basin indicate that other conditions may also allow the formation of HMSA.

REFERENCES AND NOTES

1. J. W. Munger, D. J. Jacob, M. R. Hoffmann, *J. Atmos. Chem.* **1**, 335 (1984); J. W. Munger, D. J. Jacob, J. M. Waldman, M. R. Hoffmann, *J. Geophys. Res.* **88**, 5109 (1983).
2. L. W. Richards *et al.*, *Atmos. Environ.* **17**, 911 (1983).
3. J. A. McArdle and M. R. Hoffmann, *J. Phys. Chem.* **87**, 5425 (1983); J. Hoigne, H. Bader, W. R. Haag, J. Staehelin, *Water Res.* **19**, 993 (1985).
4. G. L. Kok, S. N. Gitlin, A. L. Lazrus, *J. Geophys. Res.*, in press.
5. W. Kerp, *Arb. Kais. Gesundh.* **421**, 180 (1904).
6. L. H. Donally, *Ind. Eng. Chem. Anal. Ed.* **5**, 91 (1933).
7. U. Deister, R. Neeb, G. Helas, P. Warneck, *J. Phys. Chem.*, in press.
8. The initial formation of HMSA can be expressed in terms of gas-phase concentrations as

$$\frac{d[\mathrm{HMSA}]}{dt} = H_s H_f P_{SO_2} P_{CH_2O} \frac{1}{(1 + K_h)} \times \left(\frac{k_1 K_{a1}}{[H^+]} + \frac{k_2 K_{a1} K_{a2}}{[H^+]^2}\right)$$

9. Values for the Henry's law constants for SO_2 and CH_2O at 298 K are $H_s = 1.245M$ atm^{-1} and $H_f = 6.3 \times 10^3 M$ atm^{-1} (in terms of hydrated CH_2O). P_i is the partial pressure of species i. The acidity constants for S(IV) are $K_{a1} = 1.29 \times 10^{-2} M$ and $K_{a2} = 6.01 \times 10^{8} M$. The hydration constant for CH_2O is $K_h = 2.53 \times 10^3$. The original references and enthalpy data are given by Munger *et al.* (*1*). The rate constants are $k_1 = 7.9 \times 10^2 M^{-1}$ sec^{-1} (activation energy = 5.9 kcal mol^{-1}); $k_2 = 2.48 \times 10^7 M$ sec^{-1} (activation energy = 4.8 kcal mol^{-1}) [S. D. Boyce and M. R. Hoffmann, *J. Phys. Chem.* **88**, 4740 (1984)].
9. D. J. Jacob and M. R. Hoffmann, *J. Geophys. Res.* **88**, 6611 (1983); Y. G. Adewuyi, S-Y. Cho, R-P. Tsay, G. R. Carmichael, *Atmos. Environ.* **18**, 2413 (1984).
10. P. Warneck, W. Klippel, G. K. Moortgat, *Ber. Bunsenges. Phys. Chem.* **82**, 1136 (1978); W. Klippel and P. Warneck, *Atmos. Environ.* **14**, 809 (1980).
11. J. R. Snider and G. A. Dawson, *J. Geophys. Res.* **90**, 3797 (1985).
12. D. J. Jacob, J. M. Waldman, J. W. Munger, M. R. Hoffmann, *Tellus* **36B**, 272 (1984); D. J. Jacob, thesis, California Institute of Technology, Pasadena (1985).
13. During December 1984 and January 1985 fog water was collected at a site adjacent to the Bakersfield Airport and in Buttonwillow. Sampling commenced at the onset of fog formation and continued until the fog dissipated. Major oil fields are located within 5 km of the Bakersfield Airport in the northeast quadrant. Buttonwillow is located near the center of the valley, at least 15 km southeast of oil fields on the west side of the valley. Complete results and site descriptions are given by J. M. Waldman [thesis, California Institute of Technology, Pasadena (1985)].
14. The collector is described in D. J. Jacob, R.-F. T. Wang, R. C. Flagan, *Environ. Sci. Technol.* **18**, 827 (1984).
15. Total S(IV) was determined in an aliquot of sample that was preserved with CH_2O immediately after collection. Analysis was by the pararosaniline method [P. K. Dasgupta, K. DeCesare, J. C. Ullrey, *Anal. Chem.* **52**, 1912 (1980); P. K. Dasgupta, *ibid.* **53**, 2084 (1981)]. Standards made from Na_2SO_3 or $NaCH_2OHSO_3$ gave identical results. Analysis was complete within a week of collection; no loss of S(IV) was observed in preserved aliquots or standard solutions. Analytical error was within 5 percent.
16. Total CH_2O was determined in a separate aliquot of sample to which Nash reagent was added immediately after collection [T. Nash, *Biochem J.* **55**, 416 (1953)]. Prior to color determination, I_2 was added to destroy the S(IV) in the sample [R. V. Smith and P. W. Erhardt, *Anal. Chem.* **47**, 2462 (1975)]. Recovery of $NaCH_2OHSO_3$ standards was 90 to 100 percent compared to CH_2O standards. Minimal losses of CH_2O were observed during storage. Analytical error was less than 5 percent.
17. HMSA was determined by ion-pairing chromatography on a polystyrene divinylbenzene column (Dionex MPIC) followed by a suppressor column containing cation-exchange resin in the Ag^+ form (Dionex ISR), and a conductivity detector. The mobile phase contained 2 mM tetrabutylammonium chloride, 5 percent (by volume) CH_3OH, and $2 \times 10^{-5} M$ HCl. Analytical error was less than 5 percent. Samples to be analyzed for sulfonic acids were refrigerated, but no preservatives were used.
18. California Air Resources Board, unpublished data.
19. D. D. Reible, F. H. Shair, T. B. Smith, D. E. Lehrman, *Atmos. Environ.*, in press.

20. Supported by the California Air Resources Board (contract A4-075-32) and a summer undergraduate research fellowship from California Institute of Technology (C.T.). We thank D. Jacob, J. Waldman, D. Bucholz, and S. Hawes for their contributions to this work.

30 September 1985; accepted 30 October 1985

Geomorphic Evidence for the Distribution of Ground Ice on Mars

STEVEN W. SQUYRES AND MICHAEL H. CARR

High-resolution Viking orbiter images show evidence for quasi-viscous relaxation of topography. The relaxation is believed to be due to creep deformation of ice in near-surface materials. The global distribution of the inferred ground ice shows a pronounced latitudinal dependence. The equatorial regions of Mars appear to be ice-poor, while the heavily cratered terrain poleward of ±30° latitude appears to be ice-rich. The style of creep poleward of ±30° varies with latitude, possibly due to variations in ice rheology with temperature. The distribution suggests that ice at low latitudes, which is not in equilibrium with the present atmosphere, has been lost via sublimation and diffusion through the regolith, thereby causing a net poleward transport of ice over martian history.

DETERMINATION OF THE DISTRIBUTION of subsurface ice on Mars is critical for understanding the planet's volatile inventory and will be a major concern for future martian exploration. Many martian landforms suggest the former presence of ground ice or water, including fretted and chaotic terrain (*1*), valley systems (*2*), outflow channels (*3*), and, with less certainty, various types of patterned ground (*4*) and rampart craters (*5*). None of these landforms provides strong evidence for the present distribution, however. If sufficient ice is present now, the regolith should undergo quasi-viscous flow due to creep deformation of the ice. Accordingly, to determine where ice may be present, we have examined the approximately 24,000 Viking Orbiter images taken within 5,000 km of the surface (*6*) and mapped the distribution of three types of features—lobate debris aprons, concentric crater fill, and terrain softening—that may indicate creep of near-surface materials.

Lobate debris aprons are accumulations of erosional debris at the base of steep escarpments (*7*). Surface lineations and compressional ridges adjacent to obstacles indicate that the constituent materials have flowed away from the escarpment. Distinct convex-upward topographic profiles suggest creep deformation throughout the entire thickness of the debris apron. They are morphologically similar to terrestrial rock

S. W. Squyres, Theoretical Studies Branch, NASA Ames Research Center, Moffett Field, CA 94305.
M. H. Carr, U.S. Geological Survey, Menlo Park, CA 94025.

glaciers, which are ice-cemented accumulations of rock that flow because of ice creep (*8*). Concentric crater fill apparently develops where debris aprons are confined within impact craters, and inward flow of material produces a pattern of concentric ridges (*9*).

Terrain softening is a distinctive style of landform degradation apparent in high-resolution images. The topography in Fig. 1A is typical of what is observed at low latitudes. The terrain shows no evidence of softening. It is crisp, with sharp crater rims and slopes that are predominantly straight or concave upward in profile. The floors of the craters (except young impact craters) are generally flat and featureless. Between large craters the terrain commonly consists of rugged hills with intervening smooth areas. Sharp ridges and mesa-like hills are common. In contrast, the topography in Fig. 1B is typical of cratered terrain between latitudes 30° and 55°. Crater rim crests are rounded, and slopes are commonly convex upward. The terrain between the large craters has a smooth, rolling character and lacks the sharp ridges and hills common at low latitudes. Poleward of about ±55° the softening assumes a slightly different character, although this is less well documented because of less complete photographic coverage. Here crater rims are fairly sharp, more like those at low latitudes. The intercrater areas tend to be rougher than those at mid-latitudes, although they are not as crisp as those at low latitudes. The variations in morphology with latitude are summarized in Fig. 2.

To map the distribution of the three classes of features, we divided the planet into 1° by 1° latitude-longitude boxes, and the presence or absence of the feature was noted for each box. To avoid the effects of atmospheric obscuration, we used only images in which surface features several times smaller than the sizes of critical diagnostic features (such as the widths of crater rim crests) could be clearly distinguished. After digitizing, the data were subjected to a 3 by 3 low-pass boxcar filter for smoothing, transformed to a Mercator projection, and displayed with each type of feature mapped into one channel in a three-color (red, green, and blue) display (Fig. 3).

Virtually none of the three types of features is found within 30° of the equator. In the northern hemisphere, lobate debris aprons are most common in Tempe Fossae, Mareotis Fossae, the Phlegra Montes, in a small region of old cratered terrain north of Olympus Mons, and particularly in the fretted terrain between longitudes 280° and 0°. One lobate debris apron was found on the flanks of the shield volcano Hecates Tholus. Concentric crater fill is found in most of these areas and is also common in Utopia Planitia. In the southern hemisphere, lobate debris aprons and concentric crater fill are most common in regions adjacent to the Hellas and Argyre basins.

In the northern hemisphere, terrain softening is present in all areas where the ancient cratered highlands extend north of 30° latitude. Cratered highlands dominate the southern hemisphere, and most regions south of −30° latitude observed exhibit some degree of terrain softening. It is ubiq-

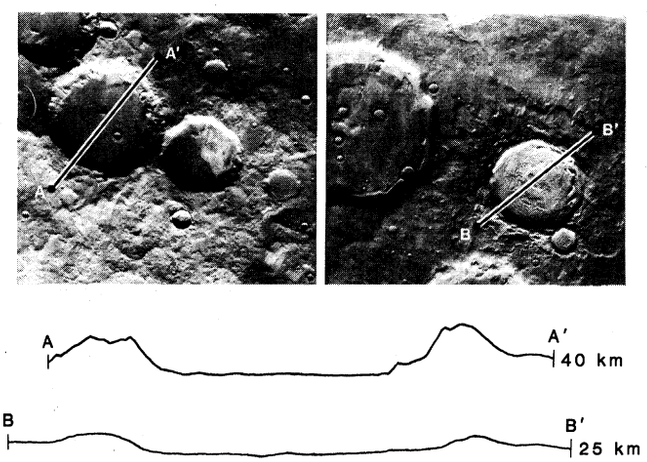

Fig. 1. Representative images of typical cratered terrain (A) and softened terrain (B) with photoclinometrically produced topographic profiles across craters. Vertical exaggeration is 4:1. The photoclinometry technique used (*20*) does not include the effects of scene-contrast reduction due to atmospheric scattering; all slopes may therefore be slightly steeper than indicated. Details of slope inflections are accurate as shown.

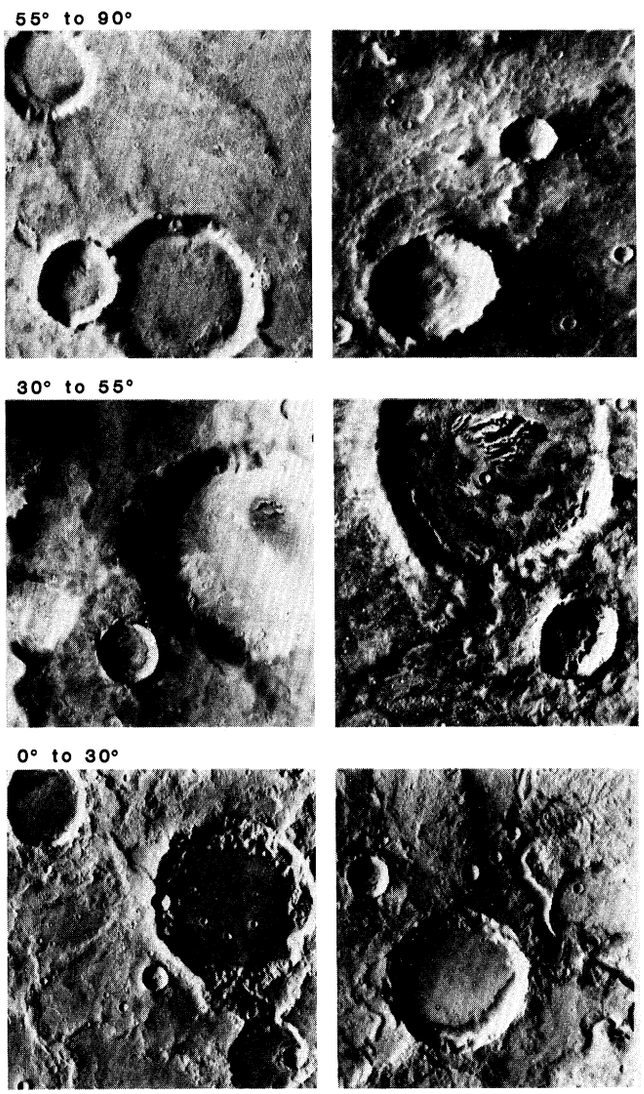

Fig. 2. Images showing the variation of cratered terrain morphology with latitude. Scale across each image is approximately 50 km.

uitous in the mid-latitudes and becomes less widespread toward the south pole.

It has been postulated that movement of lobate debris aprons is aided by creep of interstitial ice (*7*). Creep of fine-grained surface debris can occur in ice-free materials under some circumstances. On the moon, small debris aprons (<1 km) commonly occur at the base of steep slopes (*10*). However, the debris aprons on the moon are more than an order of magnitude smaller than those on Mars and do not show the flow lineations characteristic of martian lobate debris aprons and terrestrial rock glaciers. Furthermore, the distribution of martian lobate debris aprons is not uniform as that on the moon but is strongly dependent on latitude. The latitudinal dependence suggests that climatic factors are important in their development, as would be expected if ice were involved. The postulated ice within the debris apron was probably largely derived from the escarpment that was eroded to provide the debris and may have been supplemented by condensation from the atmosphere (*7*).

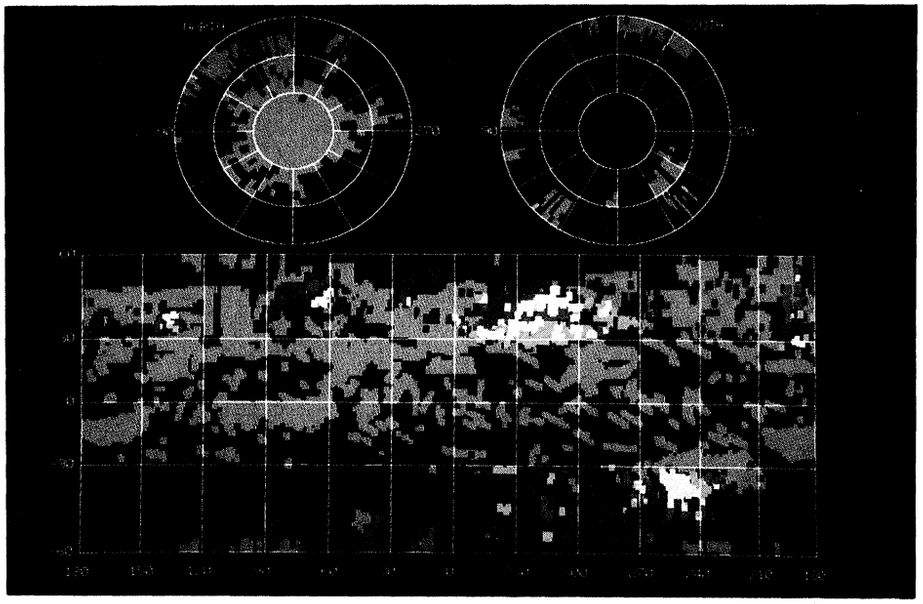

Fig. 3. Map of inferred ground-ice features on Mars. Color code: red, terrain softening; green, concentric crater fill; blue, lobate debris aprons; gray, no ground-ice features; and black, inadequate data. Where two or more features occur together, colors are added: yellow, terrain softening plus concentric crater fill; magenta, terrain softening plus lobate debris aprons; cyan, concentric crater fill plus lobate debris aprons; and white, all features.

We also considered different processes that could lead to terrain softening. Atmospheric obscuration is negligible because of our screening of the images. This is shown by Fig. 1B, in which very fine surface textures are visible in the softened terrain; clearly the perceived softening is not due to atmospheric effects. The two most likely causes of the softening are burial by eolian debris and creep of the near-surface materials. We regard creep as the probable cause. Sedimentation would leave material draped over the terrain, producing dominantly concave upward slopes and hiding sharp basal breaks in slope. The reverse is observed: slopes on crater walls tend to be convex upward, and the sharpest breaks in slope occur at the bottom of slopes rather than at rim crests, which is what is expected from creep. Also, eolian mantling would preferentially obscure small-scale knobs, pits, and impact craters, yet such features are very common in many areas of highly softened terrain. Eolian mantling does occur in many regions on Mars, as has been inferred from low- to moderate-resolution Mariner 9 images (*11*). We conclude, however, that eolian mantling clearly cannot account for the morphology observed here at high resolution. Therefore, creep is probably the dominant process contributing to terrain softening.

We argue that the latitudinal variations in creep morphology are due to the presence or absence of ground ice and to changes in the rheology of ice with latitude. Within 30° of the equator, mean surface temperatures are well above the atmospheric frost point (~200 K) at all depths (*12*). Ice is therefore unstable. Ground ice will tend to escape to the atmosphere via sublimation and diffusion through the regolith. The rate at which subsurface materials become depleted of H_2O depends on the rate of transport of vapor to the surface, which in turn depends on the diffusional permeability of the near-surface materials. For most geologic materials, diffusion rates are high compared with geologic time scales, so that depletion should occur (*13*). Unstable ice at low latitudes could only be retained over billions of years if the water vapor were prevented from reaching the surface by a compact, very fine grained regolith (*14*). At latitudes above about 40°, mean temperatures are below the frost point from depths of a few tens of centimeters to kilometers. At these latitudes and depths ice is stable. In some instances, particularly near ±30°, we observed that a thin surface layer has fractured at the crests of slope convexities, suggesting that creep has occurred at depth beneath a surface layer of low ductility and strength. This phenomenon may indicate ice depletion from only the material close to the surface.

Fanale and co-workers (*15*) have developed a model of diffusional transport of H_2O in the martian regolith. Their calculations predict long-term desiccation of equatorial regions and retention of ground ice at middle and high latitudes. The transition zone is predicted to undergo dessication near the surface, producing a wedgelike thinning of the desiccated zone and thickening of the ice-rich zone with distance from the equator. The qualitative predictions of their model are in good agreement with our observations if the features we have mapped are the result of ice-abetted creep. The agreement therefore lends further credence to the supposition that ice was involved.

At latitudes above ±55°, flow features are less developed than at latitudes from 30° to 55° (Fig. 2). This scarcity may result from a change in the rheology of the ground ice with latitude. At high latitudes, mean near-surface ground temperatures are between 160 and 200 K; at 30° latitude, temperatures are close to 215 K (*16*). The effective viscosity of ice at 160 K is higher than that at 215 K by a factor of about 8×10^4. We argue that at the lower temperatures ice flows less readily and creep of the surface materials is suppressed. The morphology at high latitudes suggests that the creep that has taken place has been restricted to a thin upper layer. Small temperature increases cause large decreases in ice viscosity, so that creep at high latitudes occurs only in a thin active layer that is affected by periods of warmer climate. It has been shown that Mars undergoes a number of variations in its orbital motion that may result in large cyclic variations in climate (*17*). The most important of these is the variation in obliquity, which has a dominant periodicity of 1.2×10^5 years. As judged from properties characteristic of terrestrial permafrost, the skin depth affected by warming over the obliquity cycle is approximately 400 m.

It is useful to compare our observed distribution with the distribution of other features that provide evidence for former ground ice and ground water on Mars. The most definitive such evidence comes from valley systems, chaotic terrain, outflow channels, and fretted terrain. Valley systems are believed to have formed by sapping and are found only in the ancient cratered terrain (*2*). They are present over a wide range of latitudes and may be weakly concentrated toward equatorial regions. Chaotic terrain and outflow channels are thought to result from melting and rapid release of large amounts of ground ice (*3*), while fretted terrain may result from more gradual release of ground ice by either melting or sublimation (*1*). All are most common at low to middle latitudes. Chaotic and fretted terrain dissect the highland materials; outflow channels, commonly arising from chaotic terrain, debouch onto the lowland plains. Crater age dating shows that outflow channel formation took place after the formation of the ancient highlands but still fairly early in martian history (*18*), while valley systems formed during the very earliest part of the planet's history (*2*). Their distributions are therefore consistent with the concept that the equatorial regions were once rich in water and ice and have subsequently been desiccated.

The origin of the ice in the martian regolith is unclear. The many lines of evidence implying that ice was common in the cratered uplands early in martian history suggest that the ice was emplaced during an early period of intense outgassing. The alternative extreme is continuous outgassing throughout the planet's history at a rate substantially lower than the low-latitude depletion rates in order to keep the low latitudes ice-free. In either case, intense early meteoritic brecciation was probably largely responsible for the apparent capability of the deep regolith to hold large amounts of water. We cannot determine what fraction of ice must be present in the near-surface materials to produce the features we have mapped. Even if only modest fractions (5 to 10 percent by volume) are present, then the data presented here suggest that the total inventory of water at the surface is close to the upper limit of the post-Viking estimates of 10 to 100 m spread evenly over the surface of the planet (*19*).

REFERENCES AND NOTES

1. R. P. Sharp, *J. Geophys. Res.* **78**, 4073 (1973); B. K. Lucchitta, *ibid.* **89**, B409 (1984).
2. D. C. Pieri, *Science* **210**, 895 (1980).
3. V. R. Baker and D. J. Milton, *Icarus* **23**, 27 (1974).
4. M. H. Carr and G. G. Schaber, *J. Geophys. Res.* **82**, 4039 (1977).
5. M. H. Carr *et al.*, *ibid.*, p. 4055. For the view that some rampart crater formation is not related to ice, see P. H. Schultz and D. E. Gault, *Lunar Planet. Sci.* **15**, 732 (1984).
6. Images with resolutions ranging from 10 to 125 m per pixel were used to map terrain softening; images with resolution as low as 500 m per pixel were used to map lobate debris aprons and concentric crater fill.
7. S. W. Squyres, *Icarus* **34**, 600 (1978).
8. C. Wahrhaftig and A. Cox, *Geol. Soc. Am. Bull.* **70**, 383 (1959).
9. S. W. Squyres, *J. Geophys. Res.* **84**, 8087 (1979).
10. T. W. Offield, U.S. Geological Survey map I-626 (1972).
11. L. A. Soderblom, T. J. Kriedler, H. Masursky, *J. Geophys. Res.* **78**, 4117 (1973).
12. C. B. Farmer and P. E. Doms, *ibid.* **84**, 2881 (1979).
13. S. M. Clifford and D. Hillel, *ibid.* **88**, 2456 (1983).
14. R. Smoluchowski, *Science* **159**, 1348 (1968).
15. F. P. Fanale, J. R. Salvail, A. P. Zent, S. E. Postawko, in preparation.
16. R. B. Leighton and B. C. Murray, *Science* **153**, 136 (1966); F. P. Fanale and R. N. Clark, in *Permafrost: Proceedings of the Fourth International Conference* (National Academy Press, Washington, DC, 1983), pp. 289–294.
17. B. C. Murray, W. R. Ward, S. C. Yeung, *Science* **180**, 638 (1973).
18. M. C. Malin, *J. Geophys. Res.* **81**, 4825 (1976); H. Masursky, J. Boyce, A. L. Dial, G. G. Schaber, M. E. Strobell, *ibid.* **82**, 4016 (1977).
19. S. I. Rasool, L. LeSargeant, *Nature (London)* **266**, 822 (1977); M. B. McElroy, Y. L. Yung, A. O. Nier, *Science* **194**, 70 (1976); M. B. McElroy, T. Y. Kong, Y. L. Yung, *J. Geophys. Res.* **82**, 4379 (1977); J. B. Pollack and D. C. Black, *Science* **205**, 56 (1979).
20. S. W. Squyres, *Icarus* **46**, 156 (1981).

21. We thank D. Maydan, K. Bilski, and A. Summers for programming assistance and C. McKay and R. Reynolds for helpful discussions. Supported by the NASA Planetary Geology and Geophysics program.

12 August 1985; accepted 11 October 1985

Human T-Cell γ Chain Genes: Organization, Diversity, and Rearrangement

THOMAS QUERTERMOUS, CORNELIS MURRE, DENO DIALYNAS, ALLAN D. DUBY, JACK L. STROMINGER, THOMAS A. WALDMAN, J. G. SEIDMAN

The human T-cell γ chain genes have been characterized in an attempt to better understand their role in immune response. These immunoglobulin-like genes are encoded in the genome in variable, joining, and constant segments. The human γ genes include at least six variable region genes, two joining segments, and two constant-region genes in germline DNA. Variable and joining segments recombine during the development of T cells to form rearranged genes. The diversity of human γ genes produced by this recombinational mechanism is greater than that produced by the murine genome but is more limited than that of other immunoglobulin-like genes.

AN ACTIVE γ GENE IS FORMED BY immunoglobulin-like rearrangement of variable (V) and joining (J) segments that occurs during somatic differentiation of T cells (*1–3*). It has been suggested that the γ chain plays a role as a cell surface receptor because of its similarities to immunoglobulin and T-cell antigen receptor α and β chains (*2–9*). However, the polypeptide chain has not yet been identified and its precise function remains uncertain. One approach to understanding the function of this molecule is to characterize the diversity of expressed γ chains. The mouse expresses a very limited number of γ chains because its genome encodes only three variable region genes. Only one of these participates in the formation of a functional gene (*3*).

There are two γ chain constant regions in the human genome that reside on the short arm of chromosome 7 (*10*). One of these constant (C) region gene segments is deleted from the genome of most human T cells. Here we report that the two C region segments are encoded about 12 kilobases (kb) apart, with at least one J region segment 5′ of each constant region. These J region segments recombine with multiple (at least three) variable region segments, suggesting that the human genome encodes more γ chain diversity than the murine genome.

To determine the structure of the human γ chain polypeptide and to obtain probes to the human V and J region segments we isolated a γ chain complementary DNA (cDNA) clone (*11*). The cDNA clone, pTγ-1, was isolated by screening a cDNA library made from the cell HPB-MLT with a DNA probe specific for the human γ chain C region (*10*). The nucleotide sequence of pTγ-1 was determined (*12*) and V, J, and C regions were identified by homology to the mouse γ gene (Fig. 1B).

The two γ chain C region genes were

T. Quertermous, Cardiac Unit, Department of Medicine, Massachusetts General Hospital, Boston 02114.
C. Murre, A. D. Duby, and J. G. Seidman, Department of Genetics, Harvard Medical School, Boston, MA 02115.
D. P. Dialynas and J. L. Strominger, Department of Biochemistry and Molecular Biology, Harvard University, Boston, MA 02138.
T. A. Waldmann, Metabolism Branch, National Cancer Institute, National Institutes of Health, Bethesda, MD 20205.